Proof of concept for turbulence measurements with the RPAS SUMO during the BLLAST campaign

Line Båserud[1], Joachim Reuder[1], Marius O. Jonassen[1,2], Stephan T. Kral[3,1,2],
Mostafa Bakhoday Paskyabi[1], and Marie Lothon[4]

[1]Geophysical Institute, University of Bergen, Allégaten 70, 5007 Bergen, Norway
[2]UNIS - The University Centre in Svalbard, 9171 Longyearbyen, Norway
[3]Finnish Meteorological Institute, Helsinki, Finland
[4]Laboratoire d'Aérologie, University of Toulouse, CNRS, France

Correspondence to: Line Båserud (line.baserud@uib.no)

Abstract.

The micro-RPAS SUMO (Small Unmanned Meteorological Observer) equipped with a five hole probe (5HP) system for turbulent flow measurements has been operated in 49 flight missions during the BLLAST (Boundary-Layer Late Afternoon and Sunset Turbulence) field campaign in 2011.
5 Based on data sets from these flights we investigate the potential and limitations of airborne velocity variance and TKE (Turbulent Kinetic Energy) estimations by an RPAS system with a take-off weight below 1 kg.

The integration of the turbulence probe in the SUMO system was still in an early prototype stage during this campaign. The main shortcomings were the use of two different, unsynchronized data
10 loggers for the 5HP flow measurements and the aircraft's attitude data required for the motion correction, and the different sampling rate for both data sets. Therefore, extensive post-processing of the data was required in order to calculate the turbulence parameters. In addition, the fine-tuning of the autopilot was not fully optimized, leading to oscillations in the vertical velocity that the motion correction routine was not able to remove. A simple block-filter has been used for the removal
15 of these oscillations. For a filter constant of 0.61 s, the SUMO data show a good agreement to sonic anemometer data for the integral parameter of σ_w, but there is still a distinct difference in the underlying energy spectrum of the data sets. Resulting estimates of TKE profiles, obtained from consecutive flight legs at different altitudes, show reasonable results, both with respect to the overall TKE level, as well as the temporal variation. A thorough discussion of the methods used and the
20 identified uncertainties and limitations of the system for turbulence measurements is included and should help the developers and users of other systems with similar problems.

1 Introduction

The understanding of the complex interaction between the vertical structure of the atmosphere and the characteristics of atmospheric turbulence is of major importance for a wide range of practical applications and for basic atmospheric research. The appropriate parameterization of turbulent exchange processes in numerical weather prediction and climate models or the estimation of structural loads in the field of engineering, e.g. for bridges or wind turbines, are prominent examples.

Profiles of Turbulent Kinetic Energy (TKE) and the underlying velocity variances of the 3-dimensional wind vector are excellent indicators for the state of ambient turbulence, as they provide information on both the absolute turbulence level and on its spatial characteristics, as e.g. local isotropy. They are also of major importance for the understanding of the TKE budget by allowing the estimation of the magnitude of TKE production and vertical transport, which are mechanisms of basic relevance for the determination of turbulent exchange in Atmospheric Boundary Layer (ABL) research.

The measurement of velocity variances requires fast-response sensors. For in-situ observations these are typically mast or tower mounted sonic anemometers or multiple-hole flow probes for airborne measurements. Mast and tower based measurements can capture the local turbulence conditions in the Surface Layer and in case of higher masts and towers also for the stable ABL as a whole. However, under convective conditions only a fraction of the ABL's vertical extent can be captured, so that important processes, in particular in the entrainment zone, cannot be observed. A few attempts have been started to extend the vertical measurement range by tethered platforms, as balloons, kites or blimps (e.g. Balsley et al., 1999; Muschinski et al., 2001; Majumdar et al., 2006; Guest, 2007). Although showing some promising results, these observational platforms require considerable infrastructure and have limitations with respect to wind speed and/or strength of convective turbulence. Remote sensing of velocity variances, e.g. by sodar (e.g. Thomas and Vogt, 1993; Gaynor, 1994; Seibert and Langer, 1996) or lidar systems (e.g. Frehlich, 2008; Pichugina et al., 2008; Sathe and Mann, 2013), is able to reach higher levels in the range of 1 km. Even though these remote sensing methods are of high value for atmospheric research, they cannot fully replace in situ observations as they have typically only limited vertical resolution and sampling rate and as the volume averaging characteristics of these methods require a number of assumptions to derive turbulence parameters for the ABL (e.g. Sjöholm et al., 2009; Sathe et al., 2011).

For these reasons direct airborne measurements by manned aircraft, providing a unique flexibility with respect to spatial sampling, have become a more popular choice for ABL turbulence investigations during the last decades (e.g. Lenschow and Stankov, 1986; Corsmeier, 2001; Lothon et al., 2007). Corresponding flow probes are either mounted directly on an exposed and undisturbed position on fixed wing aircraft or in an instrument rig towed by a Helicopter, as in the case of the Helipod (Bange et al., 2002, 2006). However, these operations are by nature logistically demanding and expensive. The rapid development of remotely piloted aircraft systems (RPAS) during the last decade has provided new airborne sensor platforms for ABL research (Elston et al., 2015) with several of

them having proven their capability for turbulence investigations (e.g. Thomas et al., 2012; Martin
60 et al., 2011; van den Kroonenberg et al., 2012; Wildmann et al., 2014). The continuous miniaturiza-
tion of electronic components and sensors, both for measurement of meteorological parameters and
the required attitude control of the aircraft's autopilot, provides now the required capability also for
micro-RPAS with a take-off weight below 1 kg (Mansour et al., 2011; Reuder et al., 2012).

The main intention of this paper is the proof of concept for measurements of velocity variance
65 and TKE from the Small Unmanned Meteorological Observer (SUMO), a micro-RPAS with a take-
off weight distinctly below 1 kg. The paper is structured as follows. Section 2 shortly describes the
RPAS SUMO with focus on the integrated five-hole probe (5HP) based turbulence measurement
system. The turbulence flights performed during the BLLAST (Boundary-Layer Late Afternoon and
Sunset Turbulence) campaign are introduced in Sect. 3, while the required data processing for the
70 calculation of turbulence parameters is described in Sect. 4. This includes the time-synchronization
of the turbulence and attitude/position data, the transformation into a meteorological coordinate sys-
tem and a filtering procedure to remove remaining oscillations in the vertical wind component. In
Sect. 5 the resulting profiles of TKE and their time-evolution are presented and discussed for differ-
ent days during the BLLAST campaign. Section 6 presents an analysis of the different uncertainties,
75 followed by a brief summary and outlook in the final Sect. 7.

2   The SUMO platform

SUMO is a micro-RPAS with a length and wingspan of 80 cm and a take-off weight of around
650 g (Reuder et al., 2009). The SUMO airframe consists of a slightly modified version of the
commercially available model aircraft FunJet from Multiplex. The system has been continuously
80 improved and developed during the last years (Reuder et al., 2012).

For navigation and flight control the system uses the open-source autopilot system Paparazzi,
which is developed and maintained under guidance by the École Nationale de l'Aviation Civile
(ENAC) in Toulouse, France (ENAC, 2008). SUMO is equipped with an inertial measurement unit
(IMU) for attitude control and uses a GPS sensor for navigation and monitoring of the aircraft's
85 position. During the BLLAST campaign the corresponding data have been acquired and stored with
10 Hz for the IMU and 4 Hz for the GPS. A more detailed description of the SUMO airframe and
the sensors used during the BLLAST campaign is given in Reuder et al. (2015).

The most recent development in instrumentation was the integration of a five-hole flow probe
(5HP) with a corresponding data computer hosting the pressure transducers and data logger (Aero-
90 probe, 2012). The Aeroprobe data computer provides airspeed, angles of attack and sideslip, and
altitude based on differential pressure measurements at a temporal resolution of 100 Hz. After cor-
recting for the aircraft's attitude and motion this enables the calculation of the 3-dimensional flow
vector at a sufficient resolution for calculation of turbulence parameters such as Turbulent Kinetic

Figure 1. The 5HP and the data computer from Aeroprobe as mounted in the SUMO airframe.

Energy (TKE). More information on the 5HP system can be found in the manual provided by the
95 manufacturer Aeroprobe (2012) and in Båserud et al. (2014).

The probe is mounted in the nose of the airframe (see Fig. 1) and is connected to the differential
pressure sensors in the data computer by six silicon tubes of about 10 cm length. The tip of the sensor
is located approximately 10 cm in front of the fuselage. Wind tunnel tests of the setup, performed
at DLR (Deutsches Zentrum für Luft- und Raumfahrt), Göttingen, Germany, in 2014, showed no
100 noticeable effects of flow distortion at this position. The angular response of the probe was tested
both stand-alone and mounted on a SUMO airframe and provided nearly identical results within the
accuracy limits of the system.

During the BLLAST campaign the 5HP data computer was not integrated into the SUMO's data
acquisition system. The 5HP flow data and the aircraft position and attitude were therefore collected
105 on different, unsynchronized data loggers with different temporal resolution. This results in certain
challenges with respect to post-processing and will be further described and discussed in Sects. 4
and 6.

3 SUMO turbulence measurements during BLLAST

The BLLAST field campaign took place from 14 June to 8 July 2011 in Lannemezan, France. The
110 main goal of the campaign was an in-depth investigation of the turbulence decay during the after-
noon transition period. A wide range of ABL instrumentation was deployed and operated in the area,
including energy balance stations, meteorological towers, radiosondes, manned aircraft, RPAS, teth-
ered balloons, and different types of remote-sensing instruments. A comprehensive overview of the
scientific goals and the campaign set-up is presented in Lothon et al. (2014).

115 The RPAS SUMO performed a total of 299 flights during the BLLAST campaign, including 49
turbulence transect flights with the 5HP. For more information on the missions the reader is referred
to Lothon et al. (2014) and Reuder et al. (2015). All turbulence flights took place in the vicinity of
the two main instrumented locations in the campaign area, Site 1 and Site 2 (Lothon et al., 2014).
The pattern for all turbulence missions during the BLLAST campaign was similar and consisted
120 of straight legs of around 1000 m length with circular turns at each end (see Figs. 2 and 3). An
overview of all turbulence flights, including the vertical levels probed, is presented in Table 1. The
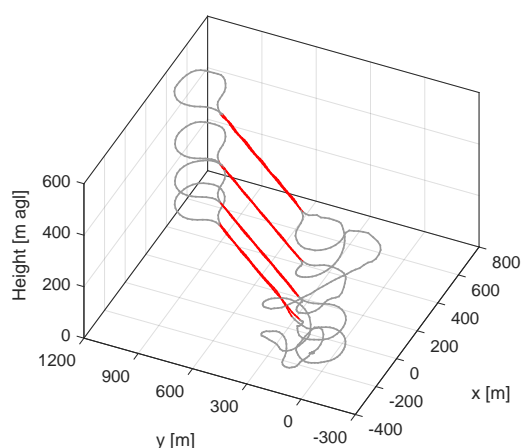
Figure 2. Typical flight pattern for the turbulence measurements from SUMO during the BLLAST campaign. Turbulence parameters are only evaluated for the straight legs (red). This example is from flight # 38 at 09:15 UTC on 27 June.
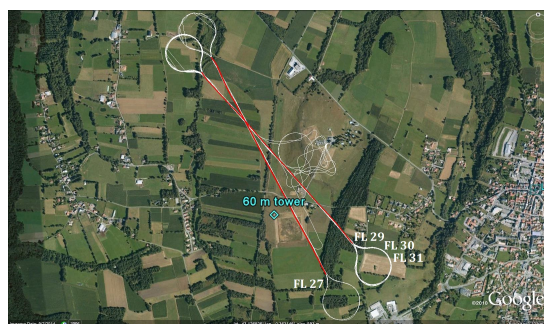
Figure 3. Flight path of the four SUMO flights (# 27, 29, 30 and 31) in the vicinity of the 60 m meteorological tower (blue diamond) situated at Site 1. The straight legs used for calculation of turbulence parameters are marked in red. Each leg is approximately 1 km long. Satellite picture from Google Earth.

battery capacity of SUMO allowed for flight missions of 20 to 25 min, corresponding to 8 to 10 straight segments. The most common flight strategies were either four legs at two different altitudes, or two legs at four different altitudes (see Fig. 2).

125   Two of the 49 flights had to be rejected due to problems with the data loggers. Several other flights had to be excluded from further analysis due to unsatisfactory time synchronization between the 5HP flow data and the IMU/GPS. A description of the corresponding synchronization procedure and the defined acceptance and rejection criteria is given in Sect. 4. Additional flights were excluded due to large deviations from the desired flight level during turbulence segments. Finally a total of 23 flights
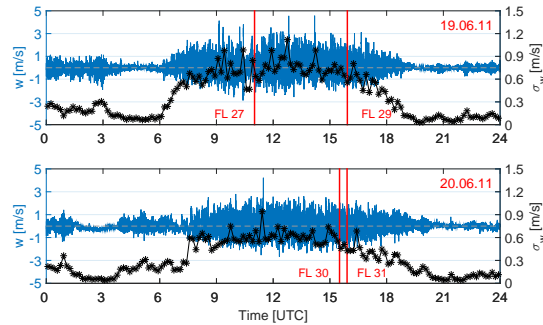
Figure 4. Sonic anemometer measurements (10 Hz) of vertical velocity, w (blue), and 10 min running mean standard deviation of vertical velocity, σ_w (black), from the 60 m meteorological tower for 19 June (top) and 20 June (bottom). The timing of the SUMO flight missions (# 27, 29, 30 and 31) is indicated by the red lines.

130   have been used for the analysis of atmospheric turbulence presented in this study. Four flights (# 27, 29, 20 and 31), performed close to the 60 m tower at Site 1 (e.g. Darbieu et al., 2015) at altitudes between 65 and 70 m (Fig. 3), have been used to compare the SUMO flow measurements with data from a 3D sonic anemometer (Campbell CSAT3) mounted at 60 m. Ten flights from 15 June (all with three to four legs at two altitudes) and 9 flights from 27 June (all with two legs at four altitudes)

135   at Site 2, have been chosen to investigate the temporal evolution of atmospheric turbulence by the means of TKE profiles (see Sect. 5).

4   Data processing

In order to transform the measured flow vector from the SUMO's turbulence system into a meteorological (earth-fixed) coordinate system with the velocity components u (positive for wind from

140   west), v (positive from south) and w (positive upward), the aircraft's attitude and velocity need to be known with high accuracy. Since the flow and IMU/GPS data relevant for this conversion were recorded on different data loggers, the first step of the post-processing was to synchronize the flow and IMU/GPS data sets in time. For this the time shift between the airspeed measured by the 5HP and the GPS ground speed was identified by a cross-correlation analysis, calculating the correlation

145   coefficient, r, as a function of the time shift. Both velocities are expected to be highly correlated, especially during flight maneuvers, such as start, landing and turns.

The synchronization procedure was applied to all turbulence flights and the result for one example is presented in Fig. 5. It shows a clear peak of above 0.99 in r for a time shift of 3.5 s. Twenty-two of the flights had an r above 0.97. Flights with $r_{max} < 0.91$ were removed from further analysis. Some

150   additional flights were ignored if a visual inspection revealed several possible time shifts giving high correlation coefficients (broad peak or prominent secondary peaks in the corresponding plots in the
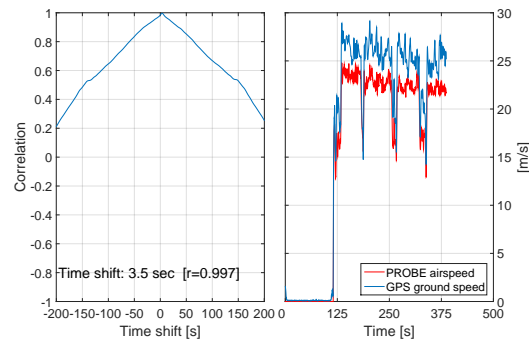
Figure 5. Example of the cross-correlation analysis between the GPS ground speed and the 5HP airspeed for one of the SUMO flights, with correlation coefficient and time shift in the left panel and time series of 5HP airspeed and GPS ground speed after synchronization in the right panel. The data are for flight # 41 on 27 June at 12:30 UTC.

left panel of Fig. 5). The time shifts were typically in the range of ± 10 s, and are related to different and varying start-up times of the 5HP data computer after switching the power on. A delayed manual start of the ground control station software after connecting the battery of the SUMO aircraft led to

155   time shifts up to 1 min in a few occasions.

Furthermore, the IMU and GPS data, which were recorded at a lower rate, were up-sampled to the 100 Hz rate of the 5HP. Potential implications of this procedure on the retrieval of turbulence parameters are discussed in Sect. 6.

Thereafter, we identified straight flight legs for our turbulence analysis based on the coordinates

160   used to define the autopilot's flight track, which are recorded during operation. This gave us an objective and automatic way to pick out the straight legs of each flight. The turbulence legs during BLLAST had a typical length of about 1000 m.

The wind speed with respect to the earth is found by performing a coordinate transformation from a Lagrangian into an Eulerian system, based on the velocity of air with reference to the aircraft

165   and the velocity and orientation of the aircraft with respect to the earth. The u, v, and w wind components in the earth coordinate system were calculated over straight flight legs based on the well established equations of Lenschow (1986). The original full set of equations include terms involving the product of angular velocities and the separation distance between the turbulence sensor and the IMU/GPS. According to Lenschow and Spyers-Duran (1989) the contribution of these terms

170   becomes insignificant if the distance is less than 10 m in case of a manned aircraft moving at a speed in the order of 100 ms^{-1}. For the SUMO system, typically moving with 20 ms^{-1}, the separation distance is about 60 cm. We have calculated the size of these additional terms for SUMO and found them to be in the order of 0.06 ms^{-1} for the vertical component, and even smaller for the horizontal
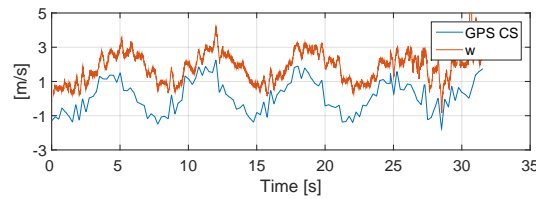
Figure 6. Example of the unfiltered vertical velocity component, w, and the GPS climb speed (GPS CS) for one single leg (about 1 km length) of flight # 38.

components, and thus too small to make any significant contribution. Consequently we are neglecting
175   these terms.

$$
u = -\frac{U_a}{(1+\tan^2\alpha+\tan^2\beta)^{1/2}}\Big[\sin\psi\cos\theta
$$
$$
+\tan\beta(\cos\psi\cos\phi+\sin\psi\sin\theta\sin\phi)
$$
$$
+\tan\alpha(\sin\psi\sin\theta\cos\phi-\cos\psi\sin\phi)\Big]+u_{gs} \tag{1}
$$

$$
v = -\frac{U_a}{(1+\tan^2\alpha+\tan^2\beta)^{1/2}}\Big[\cos\psi\cos\theta
$$
180
$$
-\tan\beta(\sin\psi\cos\phi-\cos\psi\sin\theta\sin\phi)
$$
$$
+\tan\alpha(\cos\psi\sin\theta\cos\phi+\sin\psi\sin\phi)\Big]+v_{gs} \tag{2}
$$

$$
w = -\frac{U_a}{(1+\tan^2\alpha+\tan^2\beta)^{1/2}}\Big[\sin\theta
$$
$$
-\tan\beta\cos\theta\sin\phi-\tan\alpha\cos\theta\cos\phi\Big]+w_{gs} \tag{3}
$$

In Eqs. (1–3), the 5HP airspeed is given by U_a, while the angle of attack and the angle of sideslip
185   are given by α and β, respectively. The attitude angles pitch, roll and yaw are given by θ, ϕ and ψ
respectively, and the three components of the aircraft's ground speed by u_{gs}, v_{gs} and w_{gs}. Due to
the lack of a direct measurement for ψ, we used the heading angle obtained from the GPS track for
this conversion.

After the correction for the aircraft's movement by applying the coordinate transformation (Eqs. 1–
190   3), the resulting w is frequently showing features of an oscillation, which seems to be highly corre-
lated with the time series of the vertical climb speed, altitude and pitch angle of SUMO. Figure 6
shows one example of the vertical velocity component, w, together with the GPS climb speed.

The mentioned oscillations lead to increased values of the standard deviation for the vertical wind
component, which can be seen when comparing the SUMO data to the corresponding values obtained
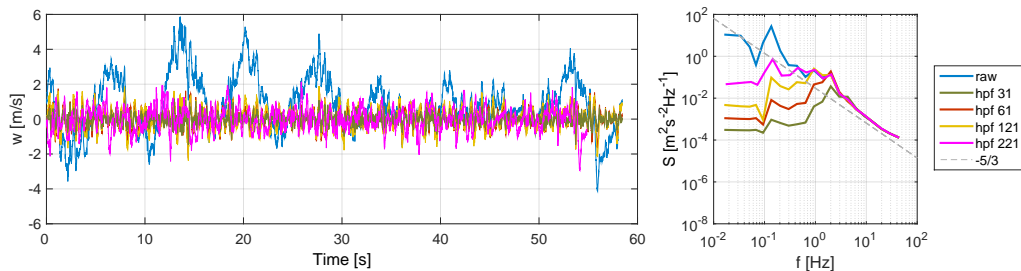
Figure 7. Example of time series (left panel) and energy spectra (right panel) of the w component from leg 2 of flight # 30 from SUMO. With unfiltered values in blue, and the four high-pass filtered (hpf) versions of w in green (running average window of 0.31 s), red (running average window of 0.61 s), yellow (running average window of 1.21 s), and magenta (running average window of 2.21 s). The -5/3 line (dashed gray) indicate the inertial subrange of the spectra.
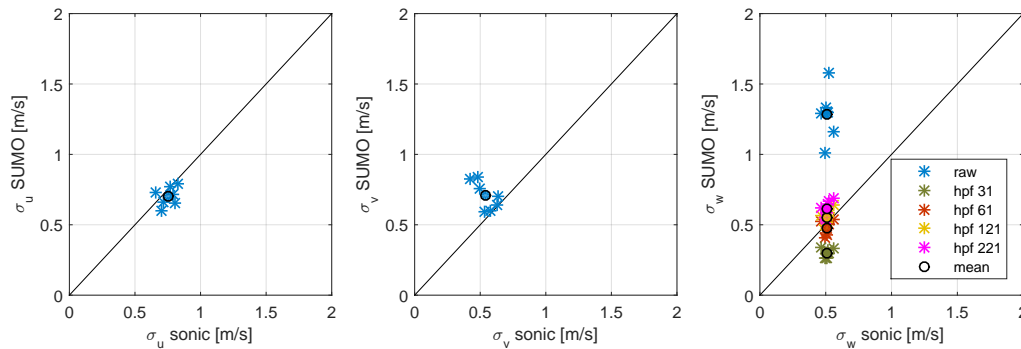
Figure 8. Standard deviations of u (left panel), v (middle panel) and w (right panel) components of the wind from SUMO (y axis) against the sonic from the 60 m meteorological tower (x axis), for all legs of flight # 30. With unfiltered values over each leg as blue stars and mean over all legs as blue circles. For the w component the resulting standard deviations after applying the four filter windows can be seen in green (window of 0.31 s), red (window of 0.61 s), yellow (window of 1.21 s) and magenta (window of 2.21 s).

195 from the sonic anemometer (Figs. 8 and 9), and thus result in unrealistic estimates of TKE (Fig. 9). As these oscillations, most likely caused by an insufficient fine-tuning of the basic control loops in the autopilot system, are a unique issue that only occured during the BLLAST campaign that has now been resolved, we decided to use a simple and pragmatic method to make the BLLAST data available for a preliminary analysis in this proof of concept study.

200   In order to remove this low frequency noise, we applied a high-pass filter (hpf) based on a running average, to the time series of w (Fig. 7). Since we want to remove a feature with a period of about 5 s, the resonable choice of filter constant will be in the order of 1 s. For a validation of the sensitivity

of the results to the averaging interval, we tested four different window sizes for this hpf. The first
running average was calculated over 0.31 s (corresponding to 31 data points), the second over 0.61 s
(corresponding to 61 data points), the third over 1.21 s (corresponding to 121 data points), and the
last over 2.21 s (corresponding to 221 data points). Figure 7 presents an example for one single leg of
flight # 30, for which the low frequency oscillations present in w are filtered by applying the different
settings mentioned above. The time series in the left panel shows that all filter constants are able to
remove the low frequency oscillations. The right panel in Fig. 7 presents the corresponding energy
spectra. This procedure was applied to the four flights in the vicinity of the 60 m meteorological
tower (see Fig. 3 for the SUMO flight tracks and the location of the tower). The wind speed and
wind direction with respect to the direction of the flight tracks (Table 2) indicate nearly pure head
and tailwind for the legs during flights # 27 and 29 and a weak side wind during flights # 30 and 31.

The results for the different filter constants were compared against the sonic anemometer data
from the tower at the corresponding height level. Figure 8 shows again flight # 30 as an exam-
ple, comparing the standard deviations from SUMO against the standard deviations from the sonic
anemometer (over a 10 min time period around each leg). The chosen 10 min averaging period
for the sonic data is based on the application of Taylor's hypothesis of 'frozen' turbulence (Taylor,
1938), i.e. the time it takes the air mass, probed by SUMO on a straight leg of around 1 km, to be ad-
vected past the stationary tower. The wind speeds were generally weak during the whole campaign,
with daily average surface winds below 2 ms^{-1} (Lothon et al., 2014). From Table 2 it is seen that
also the winds at 60 m were weak during the time of the four SUMO flights.

For σ_u and σ_v the unfiltered data from SUMO fit well with the data from the sonic, whereas the
unfiltered σ_w shows much higher values than the sonic, due to the oscillations mentioned above.
The application of the filter reduces both the overall level of σ_w as well as the spread of the data
points for the single flight legs. While the hpf 31 clearly underestimates σ_w compared to the sonic
at the mast, the three other selected filter constants lead to a reasonable agreement. Looking at the
spectral plot in the right panel of Fig. 7 it is clear that although the sonic and SUMO show a good
agreement in the integral parameter of σ_w, a distinct difference in the underlying energy spectrum of
the corresponding data sets remains. This has to be taken into account for the further interpretation
of the results. The close match in σ_w derived from SUMO to the sonic data seems to be the result
of a compensating effect between an underestimation of the low frequency contribution due to the
filtering procedure and an overestimation of the spectral energy around a peak at about 1 Hz that is
most likely related to the control algorithm of the autopilot (Reuder et al., 2015).

Figure 9 presents the comparison of σ_u, σ_v, σ_w, and TKE from SUMO to the data from the sonic
anemometer (over a 10 min time period around each leg) for all four flights in the vicinity of the
tower. The TKE from SUMO in the lower right panel of Fig. 9 is, corresponding to our previous
results, calculated using σ_u and σ_v based on unfiltered data, and σ_w based on the filtered data using
the 0.61 s running average. The resulting TKE values from both systems show a reasonable agree-
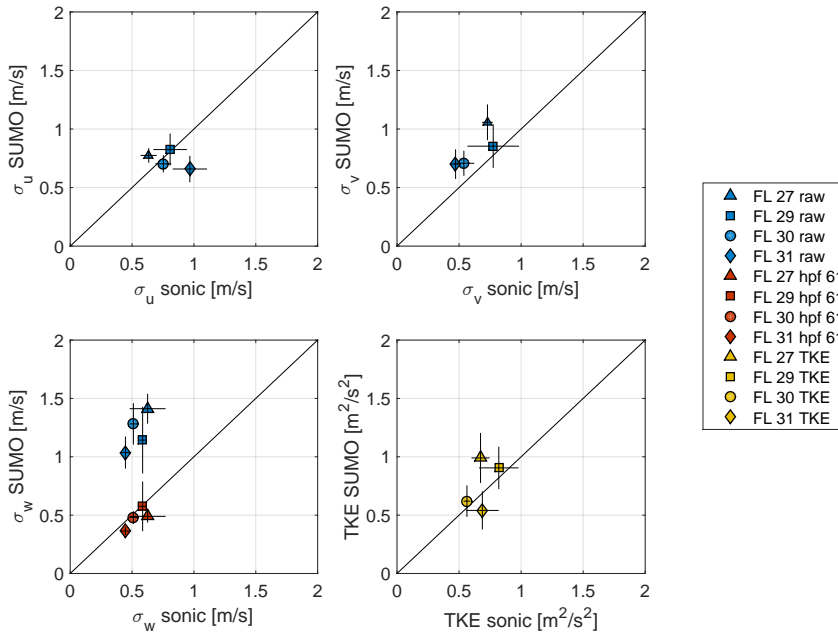
Figure 9. Mean standard deviations of u (upper left panel), v (upper right panel) and w (lower left panel) components of the wind, and mean TKE (lower right panel), from SUMO (y axis) against the sonic from the 60 m meteorological tower (x axis), for flights # 27 (triangle), # 29 (square), # 30 (circle) and # 31 (diamond). Unfiltered data can be seen in blue and the filtered data with a running window of 0.61 s in red. The resulting TKE after using unfiltered data for u and v components and filtered data for the w component is shown in yellow. The black bars show for all symbols the variation between all the straight legs within each flight.

ment for the four flights in convective conditions, with the best agreement found for flights # 29 and 30, and thus we continue to use this correction method for an estimation of TKE profiles presented in the following.

5 Results for the evolution of TKE

Nine flights at Site 2 on 27 June give the possibility to study the time evolution of TKE profiles. Seven of these flights (# 38, 40, 41, 42, 44, 46 and 47) consist of two straight legs in four different altitudes of 60, 150, 300 and 500 m above ground level (agl). An example of this type of flight pattern can be seen in Fig. 2. The remaining two flights (# 43 and 45) consist of eight and nine straight legs at one altitude of 340 m agl. Based on the results from Sect. 4, the 0.61 s running average filter has been applied to w for all of these flights. TKE was first calculated for each straight

250   leg and then averaged over all legs of the same flight at a given altitude. The resulting evolution of
the TKE profiles can be seen in Fig. 10.

The 27 June was a hot and cloud free convective day with surface temperatures reaching 30 °C.
The BL height during this day was not behaving in a 'textbook' manner. It was growing fast in the
morning, reaching a maximum of around 1200 m during a very short period around 14 UTC, before

255   decreasing again very rapidly (Lothon et al., 2014). The TKE profiles develop in parallel with this
evolution of the boundary layer height. The lowest TKE values are observed during morning and
evening, with very similar overall levels. The distinct maximum in the early afternoon is limited to
a period of less than 2 hours. Only this profile exhibits the shape of a typical TKE profile in a fully
developed CBL, with increasing values with altitude until reaching a maximum at around $1/3$ of

260   the BL height, as described e.g. by Stull (1988). The largest diurnal variation is found at 150 and
300 m agl, while the TKE values vary less in the highest and lowest levels. In particular the morning
and evening profiles show increased values in the lowest level of 60 m, indicating the importance
of shear production on TKE during these times. The profiles around noon are characterized by TKE
values that are rather constant with height.

265   Figure 11 presents the time series of TKE from ten SUMO flights during the 15 June at Site 2,
which is an example from a day with cloudy weather conditions (Lothon et al., 2014). The BL height
was growing fast in the morning and reaching values of around 1000 m around noon and remained
nearly constant for a few hours in the afternoon. Each flight during this day consisted of three to four
straight legs at both 65 and 150 m agl. During this day TKE at both levels shows a clear maximum

270   around 15 UTC before it rapidly decays throughout the afternoon. This maximum is characterized
by higher TKE values at the 150 m level, again indicating the typical shape of a TKE profile in the
developed CBL. During this period we also see the largest spread between the individual legs. For
the rest of the day the TKE values from individual legs within a flight agree more closely and also
the values for both levels are rather similar.

275   **6   Uncertainty analysis**

The SUMO system was still in a prototype stage during BLLAST when it comes to turbulence
measurements, requiring an extensive data post-processing and assumptions to be made on the way
to extract and validate the velocity variance data in 3 dimensions that are the basis for the TKE
estimation. The following section will provide a discussion of the different sources of uncertainty

280   identified and on potential pathways and suggestions to improve the situation in the future. Although
some of the issues discussed here have already been improved or solved in the further development
of the SUMO system, we expect that these methods and techniques can be valuable in a general
context, i.e. for the developers and users of other systems with similar problems.
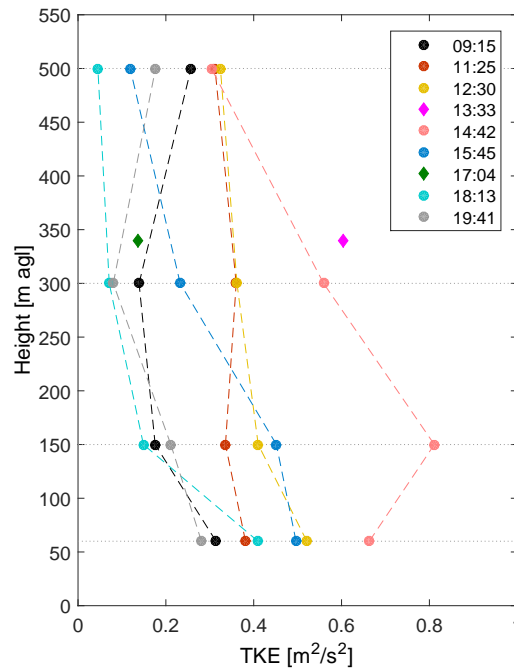
Figure 10. Profiles of TKE from 27 June at Site 2. Consecutive flights are separated by color. The average TKE value over two legs, for each altitude (60, 150, 300 and 500 m agl), is shown by the circles. For the two flights with straight legs in 340 m agl, the diamonds represent the average TKE values. The given flight times are all in UTC.

The unsynchronized data loggers of the autopilot and the turbulence probe can cause some un-
certainty. One cannot be more accurate in timing than the slowest partner, i.e. GPS (at the moment 4 Hz). The up-sampling of this GPS data and the 10 Hz attitude data can change the spectral behavior of the resulting motion corrected data sets. The latest version of SUMO uses one common data logger for the 5HP and all IMU/GPS data. For newer systems we aim to increase the IMU sampling rate to 100 Hz, and the GPS sampling rate to 10 or 20 Hz, in order to remove these issues completely.

The yaw angle (ψ) has not been measured accurately, but taken to be the angle of flight track (heading angle). This simplification might cause an error in the resulting horizontal wind components. However, it can be assumed that this does not lead to large errors as long as the aircraft's ground speed is significantly higher than the side wind component or, in other words, the straight flight legs are oriented parallel to the prevailing wind direction. Furthermore, the definition of TKE includes the variances of all three velocity components, so that errors resulting from an inaccurate yaw angle are leveled out. Following this argumentation we conclude that the assumptions made for ψ do not lead to significant errors under conditions as experienced during the BLLAST campaign,
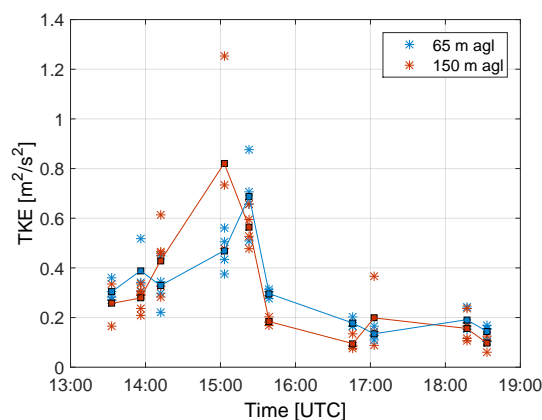
Figure 11. TKE from 15 June at Site 2. The average values of TKE over each straight leg is shown by the stars. The colors indicate the different altitudes of 65 (blue) and 150 (red) m agl. Corresponding mean TKE over all legs is shown by the squares.

as winds were weak compared to the aircraft's ground speed of around $20\,\mathrm{ms^{-1}}$. For measurements in situations with a strong cross-wind component this has, however, to be taken into account as a

300   potential error source. Furthermore, high frequency fluctuations of the yaw angle, which are not captured by the GPS heading angle, might introduce a minor uncertainty in the velocity variances and standard deviations that will then also be reflected in the TKE.

When transforming the wind vector from the aircraft to the earth-fixed coordinate system, we have neglected terms involving the product of angular velocities and the separation distance between the

305   turbulence sensor and the IMU/GPS. Tests have shown that the effects of these terms are insignificant and that the terms do definitely not compensate for the remaining oscillations in the vertical component with a period of around $5\,\mathrm{s}$.

Comparing the measurements of standard deviations and TKE from SUMO to the corresponding measurements from the sonic anemometer mounted at the $60\,\mathrm{m}$ meteorological tower may require

310   some additional considerations on the comparability of the two methods. The two basic assumptions that have to be fulfilled are Taylor's hypothesis and horizontal homogeneity. As described by Lothon et al. (2014) the area of interest was characterized by different kinds of surfaces, partially causing significant differences in the surface temperature (Reuder et al., 2015) and consequently in the surface forcing expressed by sensible and latent heat fluxes. These surface heterogeneities are likely to

315   influence the two measurement systems in different ways. The footprint at the stationary tower is only dependent on the meteorological conditions, i.e. stratification, wind speed and direction, which can be assumed to be rather constant with time. In case of the SUMO platform the footprint shows an additional dependency on the current location of the airplane, thus being more affected by surface

heterogeneity. Additional differences might arise from the horizontal distance between the flight track and the location of the tower and the different averaging procedures that have to be applied to calculate mean turbulent quantities, i.e temporal and spatial averaging. The averaging period of 10 min for the tower data does not exactly correspond to the averaging distance of 1 km of the horizontal flight legs of all flights. This choice is based on a compromise between having a long enough period for good statistics and a short enough period to ensure stationary conditions.

The most critical assumptions for the determination of the velocity variances are related to the filtering process of the remaining vertical velocity oscillations. Even after correcting for the aircraft's motion, we have to apply this method to extract realistic values for σ_w. Our choice for the filter settings is based on the comparison of four flights to sonic anemometer data, applying different settings. We are aware of the related uncertainties, e.g. the impact on the spectral characteristics of the filtered velocity components. We see a compensation of two errors, i.e. the underestimation by the filter for the low frequencies and the overestimation due to the peak at around 1 Hz, which is probably related to the control algorithm of SUMO's autopilot (Reuder et al., 2015). The fact that the results converge for four individual flights performed during two different days gives certain confidence that the selected filter parameter is also appropriate for the other turbulence flights during the BLLAST campaign. For the latest campaigns performed in 2014 on Svalbard and in the Netherlands the altitude stabilization issue of the SUMO system has been solved and is not longer a problem.

7   Summary and Outlook

We present turbulence measurements from the BLLAST field campaign, in summer 2011, obtained using the Aeroprobe 5HP system on board the micro-RPAS SUMO. This system was still in an early prototype stage during the BLLAST campaign and extensive post-processing of the resulting data was therefore needed in order to calculate the turbulence parameters. The 5HP and the aircraft attitude data loggers were not yet synchronised, for example. We solved this through cross-correlating the airspeed measured by the 5HP and the ground speed from the GPS and correcting for the corresponding time shift. Furthermore, an oscillation in the vertical wind component was discovered. This was not corrected for when converting the wind vector measurements from the aircraft reference frame to the Earth reference frame using the GPS and aircraft attitude data. Also, tests in which we applied full equations for this coordinate conversion, instead of the alternative simplified versions, did not improve the measurements in this regard. The oscillations were removed by filtering the vertical wind component using a simple high-pass filter based on a running mean. For the measurements and applications presented herein, this appears to be sufficient in the time domain, although not optimal in the frequency domain.

After post-processing, the resulting standard deviations of the three wind components, σ_u, σ_v, and σ_w, together with TKE from four SUMO flights compare favorably with measurements from

a sonic anemometer mounted at 60 m on a meteorological tower. Profiles of TKE, obtained from
consecutive flight legs at different altitudes, show low TKE values during morning and evening, and
higher TKE values during early afternoon, which would be expected given the time development in
surface forcing and corresponding ABL structure on the investigated days.

Since the BLLAST campaign, the SUMO system has been improved in several regards. The aircraft attitude and 5HP data are now synchronized on-board and logged using one single data logger.
There are no longer problems with a sub-optimal aircraft attitude (pitch) control tuning, which we
believe was the cause for the observed low-frequency oscillations in the vertical wind component
in the BLLAST dataset. Battery technology is in rapid development and new batteries have become
available since BLLAST allowing for flights lasting up to one hour. For turbulence measurements
this enables us to perform flights with either longer straight segments or an increased number of
straight segments per flight, both increasing the statistical relevance of our measurements. In addition, a fast-response temperature sensor (Wildmann et al., 2013) has been tested with the system,
allowing for the direct estimation of turbulent fluxes of sensible heat.

Still, some challenges with the system remain. Currently, the GPS heading data are used for estimating the aircraft yaw angle. For cases with weak cross-winds, such as those presented herein, this
has minor influences on the estimated turbulence parameters since the deviation from the true yaw
angle is minimal. However, for cases with strong cross-winds we have previously observed larger
deviations. To address this shortcoming in the future we are looking into possibilities of measuring
the true yaw angle directly, e.g. by magnetometers or the use of two differential GPS receivers. In
addition, the present SUMO airframe and the mounting of the 5HP exposed and unprotected in the
nose of the aircraft require an expert pilot for safe landings. In the future, alternative airframes or an
alternative mounting of the 5HP will be considered for increased user-friendliness.

As described in the introduction, the potential of the turbulence measurement capabilities of the
presented SUMO system cover a wide range of applications and extends beyond basic research on
atmospheric turbulent characteristics. Other example applications include the validation of numerical
weather prediction models, the characterization of wakes within wind farms and the estimation of
turbulent heat fluxes when the system is combined with a fast-response temperature sensor.

Acknowledgements. The BLLAST field experiment was made possible thanks to the contribution of several
institutions and supports: INSU-CNRS (Institut National des Sciences de l'Univers, Centre national de la
Recherche Scientifique, LEFE-IDAO program), Météo-France, Observatoire Midi-Pyrénées (University of Toulouse),
EUFAR (EUropean Facility for Airborne Research) and COST ES0802 (European Cooperation in Science and
Technology). The field experiment would not have occurred without the contribution of all participating European and American research groups, which all have contributed to a significant amount.
The BLLAST field experiment was hosted by the instrumented site of Centre de Recherches Atmosphériques,
Lannemezan, France (Observatoire Midi-Pyrénées, Laboratoire d'Aérologie). BLLAST data are managed by
SEDOO, from Observatoire Midi-Pyrénées.

The participation of the Meteorology Group of the Geophysical Institute, University of Bergen was facilitated
by contributions of the Geophysical Institute and the Faculty of Mathematics and Natural Sciences under the
"smådriftsmidler" scheme, a travel stipend by the Meltzer Foundation in Bergen, and the Short Term Scientific
Mission (STSM) scheme within the COST Action ES0802 "Unmanned Aerial Vehicles in Atmospheric Re-
395 search".

The authors are grateful to Anak Bhandari for the technical assistance in the preparation of the campaign, and
to Christian Lindenberg, the SUMO chief pilot during the campaign. Without his passion, determination and
patience we would never have achieved this large number of flights.

We are also grateful to Detlef Hübner from DLR (Deutsches Zentrum für Luft- und Raumfahrt) in Göttingen,
400 Germany, for facilities and technical assiatance during the wind tunnel experiments with SUMO in 2014.

References

Aeroprobe: On-The-Fly! Air Data System User's Manual Revision F, 1/2012, https://recuv-ops.colorado.edu/../OTF_Manual.pdf, 2012.

Balsley, B. B., Jensen, M. L., Frehlich, R. G., Eaton, F. D., Bishop, K. P., and Hugo, R. J.: In-situ turbulence measurement technique using state-of-the-art kite/blimp platforms, in: Proc. SPIE 3706, Airborne Laser Advanced Technology II, edited by Steiner, T. D. and Merritt, P. H., vol. 3706, pp. 2–10, doi:10.1117/12.356947, 1999.

Bange, J., Beyrich, F., and Engelbart, D. a. M.: Airborne measurements of turbulent fluxes during LITFASS-98: Comparison with ground measurements and remote sensing in a case study, Theoretical and Applied Climatology, 73, 35–51, doi:10.1007/s00704-002-0692-6, 2002.

Bange, J., Spieß, T., Herold, M., Beyrich, F., and Hennemuth, B.: Turbulent fluxes from Helipod flights above quasi-homogeneous patches within the LITFASS area, Boundary-Layer Meteorology, 121, 127–151, doi:10.1007/s10546-006-9106-0, 2006.

Båserud, L., Flügge, M., Bhandari, A., and Reuder, J.: Characterization of the SUMO Turbulence Measurement System for Wind Turbine Wake Assessment, Energy Procedia, 53, 173–183, doi:http://dx.doi.org/10.1016/j.egypro.2014.07.226, http://www.sciencedirect.com/science/article/pii/S1876610214011035, 2014.

Corsmeier, U.: Airborne turbulence measurements in the lower troposphere onboard the research aircraft Dornier 128-6, D-IBUF, Meteorologische Zeitschrift, 10, 315–329, doi:10.1127/0941-2948/2001/0010-0315, 2001.

Darbieu, C., Lohou, F., Lothon, M., Vilà-Guerau de Arellano, J., Couvreux, F., Durand, P., Pino, D., Patton, E. G., Nilsson, E., Blay-Carreras, E., and Gioli, B.: Turbulence vertical structure of the boundary layer during the afternoon transition, Atmos. Chem. Phys., 15, 10071–10086, doi:10.5194/acp-15-10071-2015, 2015.

Elston, J., Argrow, B., Stachura, M., Weibel, D., Lawrence, D., and Pope, D.: Overview of Small Fixed-Wing Unmanned Aircraft for Meteorological Sampling, Journal of Atmospheric and Oceanic Technology, 32, 97–115, doi:10.1175/JTECH-D-13-00236.1, 2015.

ENAC: Paparazzi User's Manual, http://wiki.paparazziuav.org/w/images/0/0a/Users_manual.pdf, 2008.

Frehlich, R.: Doppler lidar measurements of winds and turbulence in the boundary layer, IOP Conference Series: Earth and Environmental Science, 1, 012017, doi:10.1088/1755-1307/1/1/012017, 2008.

Gaynor, J. E.: Accuracy of sodar wind variance measurements, International Journal of Remote Sensing, 15, 313–324, doi:10.1080/01431169408954075, 1994.

Guest, P. S.: Measuring turbulent heat fluxes over leads using kites, Journal of Geophysical Research, 112, C05021, doi:10.1029/2006JC003689, 2007.

Lenschow, D.: Probing the atmospheric boundary layer, American Meteorological Society, (U.S.), 1986.

Lenschow, D. H. and Spyers-Duran, P.: Measurement Techniques: Air Motion Sensing, National Center for Atmospheric Research, Bulletin No. 23,, https://www.eol.ucar.edu/raf/Bulletins/bulletin23.html, 1989.

Lenschow, D. H. and Stankov, B. B.: Length Scales in the Convective Boundary Layer, Journal of the Atmospheric Sciences, 43, 1198–1209, doi:10.1175/1520-0469(1986)043<1198:LSITCB>2.0.CO;2, 1986.

440 Lothon, M., Couvreux, F., Donier, S., Guichard, F., Lacarrère, P., Lenschow, D. H., Noilhan, J., Saïd, F., Lacar-
rere, P., Lenschow, D. H., Noilhan, J., and Said, F.: Impact of coherent eddies on airborne measurements
of vertical turbulent fluxes, Boundary-Layer Meteorology, 124, 425–447, doi:10.1007/s10546-007-9182-9,
2007.

Lothon, M., Lohou, F., Pino, D., Couvreux, F., Pardyjak, E. R., Reuder, J., Vilà-Guerau de Arellano, J., Durand,
445 P., Hartogensis, O., Legain, D., Augustin, P., Gioli, B., Lenschow, D. H., Faloona, I., Yagüe, C., Alexander,
D. C., Angevine, W. M., Bargain, E., Barrié, J., Bazile, E., Bezombes, Y., Blay-Carreras, E., van de Boer, A.,
Boichard, J. L., Bourdon, A., Butet, A., Campistron, B., de Coster, O., Cuxart, J., Dabas, A., Darbieu, C.,
Deboudt, K., Delbarre, H., Derrien, S., Flament, P., Fourmentin, M., Garai, A., Gibert, F., Graf, A., Groebner,
J., Guichard, F., Jiménez, M. A., Jonassen, M., van den Kroonenberg, A., Magliulo, V., Martin, S., Martinez,
450 D., Mastrorillo, L., Moene, A. F., Molinos, F., Moulin, E., Pietersen, H. P., Piguet, B., Pique, E., Román-
Cascón, C., Rufin-Soler, C., Saïd, F., Sastre-Marugán, M., Seity, Y., Steeneveld, G. J., Toscano, P., Traullé,
O., Tzanos, D., Wacker, S., Wildmann, N., and Zaldei, A.: The BLLAST field experiment: Boundary-Layer
Late Afternoon and Sunset Turbulence, Atmos. Chem. Phys., 14, 10 931–10 960, doi:10.5194/acp-14-10931-
2014, 2014.

455 Majumdar, A. K., Eaton, F. D., Jensen, M. L., Kyrazis, D. T., Schumm, B., Dierking, M. P., Shoemake, M. A.,
Dexheimer, D., and Ricklin, J. C.: Atmospheric turbulence measurements over desert site using ground-based
instruments, kite/tethered-blimp platform, and aircraft relevant to optical communications and imaging sys-
tems: preliminary results, in: Proc. SPIE 6304, Free-Space Laser Communications VI, vol. 6304, p. 63040X,
doi:10.1117/12.684010, 2006.

460 Mansour, M., Kocer, G., Lenherr, C., Chokani, N., and Abhari, R. S.: Seven-Sensor Fast-Response Probe for
Full-Scale Wind Turbine Flowfield Measurements, Journal of Engineering for Gas Turbines and Power, 133,
081 601, doi:10.1115/1.4002781, 2011.

Martin, S., Bange, J., and Beyrich, F.: Meteorological profiling of the lower troposphere using the research UAV
"m2AV Carolo", Atmospheric Measurement Techniques, 4, 705–716, doi:10.5194/amt-4-705-2011, 2011.

465 Muschinski, A., Frehich, R., Jensen, M., Hugo, R., Hoff, A., Eaton, F., and Balsley, B.: Fine-Scale
Measurements Of Turbulence In The Lower Troposphere: An Intercomparison Between A Kite- And
Balloon-Borne, And A Helicopter-Borne Measurement System, Boundary-Layer Meteorology, 98, 219–250,
doi:10.1023/A:1026520618624, 2001.

Pichugina, Y. L., Tucker, S. C., Banta, R. M., Brewer, W. A., Kelley, N. D., Jonkman, B. J., and Newsom,
470 R. K.: Horizontal-Velocity and Variance Measurements in the Stable Boundary Layer Using Doppler Li-
dar: Sensitivity to Averaging Procedures, Journal of Atmospheric and Oceanic Technology, 25, 1307–1327,
doi:10.1175/2008JTECHA988.1, 2008.

Reuder, J., Brisset, P., Jonassen, M., Müller, M., and Mayer, S.: The Small Unmanned Meteorological Observer
SUMO: A new tool for atmospheric boundary layer research, Meteorologische Zeitschrift, 18, 141–147,
475 doi:10.1127/0941-2948/2009/0363, 2009.

Reuder, J., Jonassen, M., and Ólafsson, H.: The Small Unmanned Meteorological Observer SUMO: Recent
developments and applications of a micro-UAS for atmospheric boundary layer research, Acta Geophysica,
60, 1454–1473, doi:10.2478/s11600-012-0042-8, 2012.

Reuder, J., Båserud, L., Jonassen, M. O., Kral, S., and Müller, M.: Exploring the potential of the RPA system
480   SUMO for multi-purpose boundary layer missions during the BLLAST campaign, Manuscript prepared for
Atmospheric Measurement Techniques, 2015.

Sathe, A. and Mann, J.: A review of turbulence measurements using ground-based wind lidars, Atmospheric
Measurement Techniques, 6, 3147–3167, doi:10.5194/amt-6-3147-2013, 2013.

Sathe, a., Mann, J., Gottschall, J., and Courtney, M. S.: Can Wind Lidars Measure Turbulence?, Journal of
485   Atmospheric and Oceanic Technology, 28, 853–868, doi:10.1175/JTECH-D-10-05004.1, 2011.

Seibert, P. and Langer, M.: Deriving characteristic parameters of the convective boundary layer from
sodar measurements of the vertical velocity variance, Boundary-Layer Meteorology, 81, 11–22,
doi:10.1007/BF00119396, 1996.

Sjöholm, M., Mikkelsen, T., Mann, J., Enevoldsen, K., and Courtney, M.: Spatial averaging-effects on
490   turbulence measured by a continuous-wave coherent lidar, Meteorologische Zeitschrift, 18, 281–287,
doi:10.1127/0941-2948/2009/0379, 2009.

Stull, R.: An Introduction to Boundary Layer Meteorology, Springer, 1988.

Taylor, G. I.: The Spectrum of Turbulence, Proceedings of the Royal Society of London A: Mathematical,
Physical and Engineering Sciences, 164, 476–490, doi:10.1098/rspa.1938.0032, 1938.

495 Thomas, P. and Vogt, S.: Intercomparison of turbulence data measured by SODAR and sonic anemometers,
Boundary-Layer Meteorology, 62, 353–359, doi:10.1007/BF00705564, 1993.

Thomas, R. M., Lehmann, K., Nguyen, H., Jackson, D. L., Wolfe, D., and Ramanathan, V.: Measurement of
turbulent water vapor fluxes using a lightweight unmanned aerial vehicle system, Atmospheric Measurement
Techniques, 5, 243–257, doi:10.5194/amt-5-243-2012, 2012.

500 van den Kroonenberg, A. C., Martin, S., Beyrich, F., and Bange, J.: Spatially-Averaged Temperature Struc-
ture Parameter Over a Heterogeneous Surface Measured by an Unmanned Aerial Vehicle, Boundary-Layer
Meteorology, 142, 55–77, doi:10.1007/s10546-011-9662-9, 2012.

Wildmann, N., Mauz, M., and Bange, J.: Two fast temperature sensors for probing of the atmospheric boundary
layer using small remotely piloted aircraft (RPA), Atmospheric Measurement Techniques, 6, 2101–2113,
505   doi:10.5194/amt-6-2101-2013, 2013.

Wildmann, N., Ravi, S., and Bange, J.: Towards higher accuracy and better frequency response with standard
multi-hole probes in turbulence measurement with remotely piloted aircraft (RPA), Atmospheric Measure-
ment Techniques, 7, 1027–1041, doi:10.5194/amt-7-1027-2014, 2014.

Table 1. All SUMO turbulence transects performed during the BLLAST campaign. The flights used for further analysis are shown in bold. The abbreviation 'sshs' refers to the 'small-scale heterogeneity site' located at Site 1.

#	Date	Time	Site	Alt [m agl]	Comments
1	13.06	14:50	1	150,100,65	NNE-SSW
2	13.06	15:14	1	65,100,150	NNE-SSW
3	13.06	16:46	1	150,100,65	NNE-SSW
4	13.06	17:11	1	65,100,150	NNE-SSW
5	14.06	12:15	1	150,100,65	NNE-SSW
6	14.06	12:35	1	65,100,150	NNE-SSW
7	15.06	07:22	1	150,65	NNE-SSW
8	15.06	07:37	1	65,150	NNE-SSW
9	15.06	09:50	1	150,65	NNE-SSW
10	15.06	10:04	1	65,150	NNE-SSW
11	15.06	13:15	2	140,85	moor
12	**15.06**	**13:32**	**2**	**65,150**	**moor**
13	**15.06**	**13:56**	**2**	**150,65**	**moor**
14	**15.06**	**14:12**	**2**	**65,150**	**moor**
-	15.06	14:47	2	150,65	logg fail
15	**15.06**	**15:03**	**2**	**65,150**	**forest**
16	**15.06**	**15:23**	**2**	**150,65**	**fields S**
17	**15.06**	**15:39**	**2**	**65,150**	**fields S**
18	15.06	15:59	2	150,65	fields N
19	15.06	16:17	2	65,150	fields N
20	**15.06**	**16:45**	**2**	**150,65**	**fields N**
21	**15.06**	**17:03**	**2**	**65,150**	**fields N**
22	15.06	17:24	2	150,65	fields N
23	**15.06**	**18:17**	**2**	**150,65**	**fields N**
24	**15.06**	**18:33**	**2**	**65,150**	**fields N**
25	17.06	12:51	1	65	N-S sshs
26	17.06	13:32	1	65,150	survey sshs
27	**19.06**	**10:50**	**1**	**65**	**NW-SE**
28	19.06	13:31	1	60	NW-SE
29	**19.06**	**15:46**	**1**	**65**	**NW-SE**
30	**20.06**	**15:21**	**1**	**70**	**NW-SE**
31	**20.06**	**15:40**	**1**	**70**	**NW-SE**
32	25.06	17:25	2	60	moor
33	25.06	17:47	2	80	forest
34	26.06	11:32	2	60,150,300,500	moor
35	26.06	11:49	2	80	forest
36	26.06	14:31	2	60,150,300,500	moor
37	26.06	19:30	2	1000,750,500,300	moor
-	27.06	08:09	2	80,150,300,500	logg fail
38	**27.06**	**09:15**	**2**	**60,150,300,500**	**moor**
39	27.06	10:17	2	60,150,300,500	moor
40	**27.06**	**11:25**	**2**	**60,150,300,500**	**moor**
41	**27.06**	**12:30**	**2**	**60,150,300,500**	**moor**
42	**27.06**	**13:32**	**2**	**60,150,300,500**	**moor**
43	**27.06**	**14:42**	**2**	**340**	**moor**
44	**27.06**	**15:45**	**2**	**60,150,300,500**	**moor**
45	**27.06**	**17:04**	**2**	**340**	**moor**
46	**27.06**	**18:12**	**2**	**60,150,300,500**	**moor**
47	**27.06**	**19:41**	**2**	**60,150,300,500**	**moor**

Table 2. SUMO turbulence transects near the 60 m tower. Wind direction (WD) and wind speed (WS) are based on 10 min average values from the sonic anemometer mounted at 60 m.

#	Legs	Track [°]	WD [°]	WS [ms^{-1}]
27	6	330/150	350	1.6
29	4	320/140	317	3.6
30	7	320/140	43	2.3
31	9	320/140	53	2.7